INTERNATIONAL JOURNAL OF PRECISION ENGINEERING AND MANUFACTURING Vol. 17, No. 5, pp. 565-577 MAY 2016 / 565
DOI: 10.1007/s12541-016-0069-x ISSN 2234-7593 (Print) / ISSN 2005-4602 (Online)

Integrated Model-based Backstepping Control for an Electro-Hydraulic System

Dang Xuan Ba[1], Kyoung Kwan Ahn[2,#], Dinh Quang Truong[2], and Hyung Gyu Park[2]

1 School of Mechanical Engineering, Graduate School, University of Ulsan, 93, Daehak-ro, Nam-gu, Ulsan, 44610, South Korea
2 School of Mechanical Engineering, University of Ulsan, 93, Daehak-ro, Nam-gu, Ulsan, 44610, South Korea
Corresponding Author / E-mail: kkahn@ulsan.ac.kr, TEL: +82-52-259-2282, FAX: +82-52-259-1680

KEYWORDS: Electro-hydraulic system, Backstepping control, Nonlinear control, Integrated control, Model-based control

The demand to obtain an accurate and high efficiency hydraulic actuator has been increasing in heavy industries. However, the existence of uncertain, nonlinear, and unknown terms in system dynamics limits the performance of the hydraulic actuator significantly. To deal with these problems, this paper proposes an advanced control approach, named the integrated model-based backstepping (IBS) controller, for position-tracking control of a pump-controlled Electro Hydraulic System (PEHS). First, a mathematical model of the studied system is fully derived in which the structure of the system elements is clearly presented. Second, to realize the control performance in both transient and steady-state responses, and to simplify the design procedure, an advanced backstepping technique is then employed to compensate for the nonlinearities and unknown terms, while the uncertainties are well treated by a novel identification method based on the obtained model. Third, the stability of the closed-loop system is theoretically maintained using Lyapunov functions. Finally, the effectiveness and feasibility of the proposed method are confirmed by comparing with a tuned proportional-integral-derivative (PID) controller and a direct backstepping (DBS) controller in the real-time tracking control of the PEHS to follow various trajectories under different testing conditions.

Manuscript received: August 3, 2015 / Revised: November 17, 2015 / Accepted: December 30, 2015

NOMENCLATURE

x = displacement of the main cylinder or system position
P_1 = pressure in chamber 1 of the main cylinder
P_2 = pressure in chamber 2 of the main cylinder
Q_1 = flow rate at chamber 1 of the main cylinder
Q_2 = flow rate at chamber 2 of the main cylinder
Q_{cLi} = internal leakages of the main cylinder
C_{cLi} = coefficient of internal leakages of the main cylinder
Q_{cLe1} = external leakages at chamber 1 of the main cylinder
Q_{cLe2} = external leakages at chamber 2 of the main cylinder
A_1 = effective area at chamber 1 of the main cylinder
A_2 = effective area at chamber 2 of the main cylinder
d_t = stroke length of the main cylinder
Q_{1p} = supply flow at side 1 of the pump
Q_{2p} = supply flow at side 2 of the pump
Q_{pLi} = internal leakages of the pump
C_{pLi} = coefficient of internal leakages of the pump
Q_{pLe1} = external leakages at side 1 of the pump
Q_{pLe2} = external leakages at side 2 of the pump
D = pump displacement
w = pump speed
η_V = volumetric efficiency of the pump
J_{HP} = inertia moment of the pump
T_{fHP} = coefficient of viscous friction torque of the pump
K_{dr} = driver gain
u = input voltage supplied to driver
M = total mass effecting to the system motion
β_e = effective bulk modulus of the hydraulic fluid
$\hat{\bullet}$ = estimate of $\bullet$
$\tilde{\bullet} \triangleq \hat{\bullet} - \bullet$ = estimation error of $\bullet$
$\bullet_{max}$ = maximum value of $\bullet$
$\bullet_{min}$ = minimum value of $\bullet$
$\upsilon_\bullet \triangleq \bullet_{max} - \bullet_{min}$ = width of the feasible range of $\bullet$
$\Delta_\bullet \triangleq \sup(|\bullet|)$ = supreme absolute value of $\bullet$

$R_{f_{i|i\triangleq 0..4.}}$ = estimation rate matrices

$l_{i|i\triangleq 2,3.}$ = estimation error gains

$f_{i|i\triangleq 0..4.}$ = uncertain functions

$\Upsilon_{i|i\triangleq 0..4.}$ = certain vectors extracted from the uncertain functions

$\Xi_{i|i\triangleq 0..4.}$ = uncertain vectors extracted from the uncertain functions

$\nu_{i|i\triangleq 0..4.}$ = unknown terms extracted from the uncertain functions

δ = modeling error

1. Introduction

Electro-hydraulic system (EHS) has become increasingly more popular in modern industries, especially heavy industries and airplane manufacturing, due to ability of high force generation. Many EHS applications have been commercialized such as in press machines,[1] excavators,[2] and track cranes.[3] Basically, electro-hydraulic systems can be divided into two main types: valve-controlled EHS and pump-controlled EHS, tagged as VEHS and PEHS, respectively. The configuration of a VEHS usually consists of a high-pressure fluid supplier and a main actuator. The pressure of the supplier is normally maintained at a fixed value and the actuator operation is based on the valve adjustment.[4,5] Although a fast response can be easily obtained with this system, a great deal of system energy can be lost at the control valve due to the throttle phenomenon. In order to address this problem, pump-controlled systems have been introduced as feasible solutions.[1,6,7] Here, the motion of a PEHS is controlled directly by the operation of the pump. Hence, the lost energy is reduced significantly. However, complications in both design and control are the main drawbacks of this type of system.

Many techniques have been developed for accurate position (or force) control of electro-hydraulic systems. First, proportional-integral-derivative (PID) and advanced PID approaches need to be discussed.[8-10] PID gains have been derived using many methods, such as genetic algorithm, fuzzy technique, and model-based analysis, to achieve remarkable results. Nevertheless, since the control decision was produced only from the control error, it was difficult to maintain good performance in different working conditions. Moreover, the closed-loop stability of such controllers was not proven. To address this limitation, linear methods[11-13] and linearized techniques[14,15] have been introduced. Yu et al.[16] constructed an indirect adaptive controller from parameter estimation and a linear pole placement design. The employed controller demonstrated better performance than that of the suboptimal PID controllers. However, relying on linear models of plants, which contain large numbers of complexities and nonlinearities,[17] certainly restricts the control efficiency. Thus, another category of adaptive nonlinear controllers has been proposed with the use of full mathematical nonlinear models. Through the adaptive sliding mode[18] and backstepping[19,20] controllers, parametric uncertainties of the controlled system were estimated by adaptation laws and the nonlinearities (and uncertain nonlinearities) were maintained by robust nonlinear designs. Although the performances were significantly improved, the adaptation laws were only applied to the last state of the mathematical models. In fact, uncertainties exit in all states of the systems. Furthermore, integrated direct/indirect methods[21-23] were employed to control such systems. All uncertain parameters of the systems were identified online using least-squares (LS) algorithm and were then fed to the nonlinear controllers separately to improve the performances. Nonetheless, the LS method is not an ideal option for models containing unknown elements. In particular, focusing on cylinder-actuated systems using PEHSs, many problems remain with the complete modeling of these systems.[19,24] For example, supplement flows to compensate for different chamber volumes through check valves were considered as parametric uncertainties.[19] In fact, these terms are used as highly nonlinear functions. Besides, other unknown terms which are related to load variation, system modeling error, noise, sensor tolerant and friction, etc., were not studied or simplified in the existing methods.[18,20] These issues could cause a chatting problem or a high steady-state control error.

In order to overcome the above mentioned drawbacks, the aim of this article is to develop an advanced nonlinear controller for accurate position-tracking of a typical PEHS. First, the system mathematical model is fully derived. The system dynamics are here explored more comprehensively than in the previous literature. The supplement flows are analyzed as a combination of uncertainties, nonlinearities, and unknown elements. These unknown elements are also divided into two parts: uncertainty and a smaller unknown term. Based on the proposed model, a novel identification method is proposed to estimate the uncertain parameters accurately. An equivalent model of the studied system with estimation error gains is then utilized to run online with the real system. Second, to deal with the nonlinearities and unknown terms for a good tracking performance, a smooth robust state control method is proposed. The system states are divided into trivial states and crucial states. The trivial states are composited into a new virtual state using the Rough-Hurwitz stability criterion. Next, both the virtual state and the crucial states are controlled by the backstepping theory. Furthermore, some advanced functions are added to the controller to enhance both transient and steady-state responses, while linear robust terms are employed to avoid the chattering problem. To increase the excitation ability of the estimation procedure in the control process, the model-based identification method is also integrated into the controller. Third, convergence of the identification method and stability of the closed-loop control system are theoretically maintained via Lyapunov functions. Finally, an experimental apparatus using the researched PEHS is set up. Real-time experiments are then performed on this system under different working conditions to verify the feasibility of the designed controller. Additionally, a comparative study with a tuned PID controller[25] and a direct backstepping (DBS) controller[19] is implemented on the same system and testing conditions to convincingly demonstrate the effectiveness of the proposed approach.

The remainder of the paper is organized as follows: the studied PEHS and its model are clearly described in Section 2; the controller design and novel identification theory are explored in Section 3; Section 4 shows the experimental setups, control results and discussion and; the conclusions and future research are presented in Section 5.

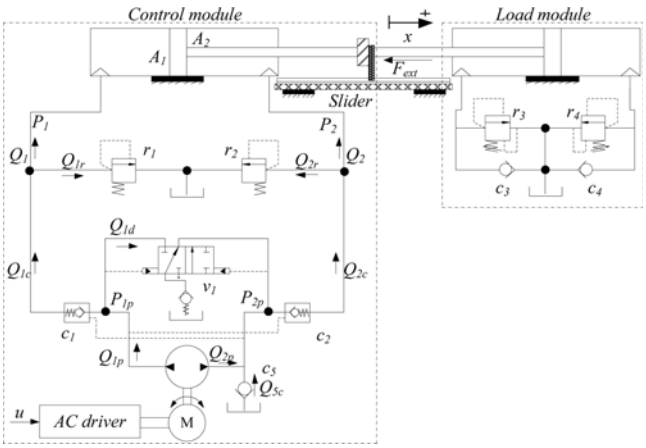

Fig. 1 Working principle of the studied system

2. System Modeling and Problem Statements

To increase the energy efficiency, the researched system is designed based on the working principle of a pump-controlled EHS and delineated as the control module in Fig. 1. The system motion is generated by a double-acting single-rod cylinder (DAJON TECH, D140H-SD50B-N300), which is simple in design, convenient for installation, and widely used in industrial applications. A fixed displacement bidirectional hydraulic gear pump (GALTECH, 2SM-G-4-R-SAEA-13GGA-VT) is employed to actuate the cylinder via a hydraulic control circuit. The pump speed is regulated by controlling an AC servo motor (HIGEN, FMACN10-AB00) using a proper driver (HIGEN, FDA7010).

In addition, to create loading conditions for the PEHS tests, a load module is attached to the right side of the system as shown in Fig. 1. Here, the load part is another similar cylinder incorporated with a passive hydraulic circuit employing pressure relief functions and check valves. The loading condition is therefore altered by manually adjusting the cracking pressure of the two relief valves (WINNER RD-08W-20WL).

By applying Newton's second law, the position dynamics of the system can be presented

$$M\dot{x} = P_1A_1 - P_2A_2 - F_{ext} - F_l(\dot{x}) \tag{1}$$

where F_{ext} is the external force and F_l is lumped uncertain nonlinearities such as viscous friction, static friction, Coulomb friction, and hard-to-model terms.[5,26]

The pressure dynamics inside the cylinder chambers can be written as[26,27]

$$\begin{cases} \dot{P}_1 = \dfrac{\beta_e}{V_{10}+A_1x}(Q_1 - A_1\dot{x} - Q_{cLi} - Q_{cLe1}) \\ \dot{P}_2 = \dfrac{\beta_e}{V_{20}-A_2x}(Q_2 + A_2\dot{x} + Q_{cLi} - Q_{cLe2}) \end{cases} \tag{2}$$

Here, V_{10} and V_{20} are the original total volumes in which each volume includes the initial volume of a cylinder chamber and the volume of the corresponding pipelines connecting to this chamber.

From the designed hydraulic circuit, the supply flows to the chambers are calculated separately as

$$\begin{cases} Q_1 = Q_{1p} - Q_{1d} - Q_{1r} \\ Q_2 = Q_{2p} + Q_{2d} - Q_{2r} \end{cases} \tag{3}$$

where Q_{1d}, Q_{1r}, and Q_{2r} are the discharged flows through the directional valve and the relief valves. Q_{5c} is the charged flow from the tank through the check valve c_5. Note that the values of Q_{1r} and Q_{2r} are zero in normal working condition because these relief valves are overpressure protectors.

The pump flows (Q_{1p} and Q_{2p}) can be presented as linear functions as follows[19]

$$\begin{cases} Q_{1p} = \eta_V Dw - Q_{pLi} - Q_{pLe1} \\ Q_{2p} = -\eta_V Dw + Q_{pLi} - Q_{pLe2} \end{cases} \tag{4}$$

Assumption 1:

a) The hydraulic energy is not lost on the transferred pipelines.

b) All external leakages are neglected:

$$Q_{cLe1} = Q_{cLe2} = Q_{pLe1} = Q_{pLe2} = 0 \tag{5}$$

c) The used hydraulic fluid is incompressible. Hence, the flows of the directional valve and check valve can be approximated as

$$\begin{cases} Q_{1d} \triangleq Q_{1de} + \delta_{1d} = -\dot{x}(A_1 - A_2)sm(-\dot{x}) + \delta_{1d} \\ Q_{5c} \triangleq Q_{5ce} + \delta_{5c} = \dot{x}(A_1 - A_2)sm(\dot{x}) + \delta_{5c} \end{cases} \tag{6}$$

where Q_{1de}, δ_{1d} and Q_{5ce}, δ_{5c} are the nominal functions and modeling errors of Q_{1d} and Q_{5c}, respectively, and $sm(*)$ is a log-sigmoid function[21] which is defined as

$$sm(*) = \frac{1}{1+e^{-\lambda_1 *}} \quad \text{where} \quad \lambda_1 > 0 \tag{7}$$

d) All internal leakage flows are laminar. The flows can be calculated as[25]

$$\begin{cases} Q_{cLi} = C_{cLi}(P_1 - P_2) \\ Q_{pLi} = -\dfrac{4\pi^2 C_{pLi}}{\mu_V D}(J_{HP}\dot{w} + T_{fHP}w + \delta_p) \end{cases} \tag{8}$$

e) The zero point is determined directly in the middle of the cylinder. The working position of the system is in a range of

$$x \in \left[-\frac{d_t}{2};\ \frac{d_t}{2}\right] \tag{9}$$

The original control volumes are subsequently followed by

$$\begin{cases} V_{10} = V_{1p} + A_1\dfrac{d_t}{2} \\ V_{20} = V_{2p} + A_2\dfrac{d_t}{2} \end{cases} \tag{10}$$

where V_{1p}, V_{2p} are the volumes of the pipelines and unused zones at chamber 1 and chamber 2, respectively.

f) The controller inside the motor driver is sufficiently good such that the pump speed can be expressed by a linear function of input voltage:

$$w = K_{dr}\,u \tag{11}$$

g) Hysteresis time of the system is smaller than the sampling time.

By defining state variables as $X \triangleq [x_1\ x_2\ x_3]^T = [x\ \dot{x}\ (P_1A_1 - P_2A_2)]^T$ and combining Eqs. (1)~(11), the system dynamics can be summarized in state-space form as

$$\begin{cases} \dot{x}_1 = x_2 \\ \dot{x}_2 = \dfrac{1}{M}(x_3 - (F_{ext} + F_l(\dot{x}))) \\ \dot{x}_3 = \dfrac{1}{f_4(x_1)}(f_2(x_1, x_2, P_1, P_2) + \delta_2 + f_3 u) \end{cases} \tag{12}$$

where

$$\begin{cases} f_2 = A_1(V_{20} - A_2x_1)(-A_1x_2 - C_{cLi}(P_1 - P_2) + x_2(A_1 - A_2)sm(-x_2)) \\ \quad -A_2(V_{10} + A_1x_1)(A_2x_2 + C_{cLi}(P_1 - P_2) + x_2(A_1 - A_2)sm(x_2))) \\ \quad +(A_1(V_{20} - A_2x_1) + A_2(V_{10} + A_1x_1))\dfrac{4\pi^2 C_{pLi}}{\eta_v D}J_{HP}\dot{w} \\ \delta_2 = -A_1(V_{20} - A_2x_1)\left(\delta_{1d} - \dfrac{4\pi^2 C_{pLi}}{\eta_v D}\delta_p\right) \\ \quad -A_2(V_{10} + A_1x_1)\left(\delta_{5c} - \dfrac{4\pi^2 C_{pLi}}{\eta_v D}\delta_p\right) \\ f_3 = \left(\eta_v D + T_{fHP}\dfrac{4\pi^2 C_{cLi}}{\eta_v D}\right)K_{dr}(A_2V_{10} + A_1V_{20}) \\ f_4 = \beta_e^{-1}(V_{10} + A_1x_1)(V_{20} - A_2x_1) \end{cases} \tag{13}$$

Remark 1:

The obtained model shows that the studied system is an uncertain nonlinear system. F_{ext}, F_l are unknown functions. δ_{1d}, δ_{5c}, and δ_p are the non-modeled elements. C_{cLi}, C_{pLi} are difficult to be determined exactly. V_{10}, V_{20}, and M are also uncertain. In addition, η_V and β_e can change during the working process. Hence, designing an accurate position-tracking controller for the unknown uncertain nonlinear system is a considerable challenge.

3. Integrated Controller Design

In this section, a nonlinear controller is designed to control the system output x tracking to the desired profile x_d as closely as possible by covering all uncertain, nonlinear, and unknown terms of the system based on the results obtained from Section 2. The controller is developed based on an advanced procedure of backstepping technique.

Assumption 2:

a) From the studied configuration as shown in Fig. 1, the external force could be considered as a mass-damping system[4] of uncertain parameters and a smaller unknown element:

$$F_{ext} = b_1x + b_2\dot{x} + \delta_{11} = b_1x_1 + b_2x_2 + \delta_{11} \tag{14}$$

b) The flumped uncertain force is divided into viscous friction, and static friction forces,[21,26] and another unknown term:

$$F_l = b_3\dot{x} + b_4\tanh(\dot{x}) + \delta_{12} = b_3x_2 + b_4\tanh(x_2) + \delta_{12} \tag{15}$$

Here, the external force and friction force can be synthesized to a new function as

$$\begin{aligned} F_{ext} + F_l &= b_1x_1 + (b_2 + b_3)x_2 + b_4\tanh(x_2) + \delta_{11} + \delta_{12} \\ &\triangleq -f_1 + \delta_1 \end{aligned} \tag{16}$$

where $\tanh(*) = \dfrac{1 - e^{-\lambda_2 *}}{1 + e^{-\lambda_2 *}}e$ and $\lambda_2 > 0$.

c) The change of all uncertain parameters is much slower than that of the sampling time.

d) The system variables $x_{i|i\triangleq 1,2,3.}$ can be measured with the given tolerances $\sigma_{i|i=1,2,3}$.

e) Boundaries of all uncertain parameters and unknown elements are known.

The full state-space form Eq. (12) of the studied system can be rewritten as

$$\begin{cases} f_0\dot{x}_2 = x_3 + f_1 + \zeta_2 \\ \dot{x}_3 = \dfrac{1}{f_4}(f_2 + f_3u + \zeta_3) \end{cases} \tag{17}$$

where $f_0 \triangleq M$; and ζ_2, ζ_3 are the lumped unknown terms combined from the measured errors, load variation modeling errors, and hydraulic modeling errors. These terms are obviously bounded.

3.1 Nonlinear controller

Assumption 3:

a) The desired reference input is bounded and its time derivatives are also bounded up to the third order.

b) All uncertain parameters and unknown elements are bounded in the convex sets in which their center points are fixed and bounded. These boundaries are also known.

Consider a composited control error created from the control objective $e = x_1 - x_d$ and a positive constant k_1 as follows

$$s = k_1e + \dot{e} \tag{18}$$

The time derivative of the error using the system Eq. (17) is given

$$\dot{s} = \frac{1}{f_0}(x_3 + f_1 + \zeta_2) - \ddot{x}_d + k_1\dot{e} \tag{19}$$

As seen in Eq. (18), when the value of k_1 is chosen to be greater than 1, a good control result e will be obtained from a large value of the error s. Hence, in order to control the error to be as small as possible, a virtual control input is chosen as

$$x_{3d} = \hat{f}_0(\ddot{x}_d - k_1\dot{e}) - \hat{f}_1 - k_2s - s_s \tag{20}$$

where k_2 is a positive constant and s_s is a bounded function of s.

Here, if $\hat{f}_0$, $\hat{f}_1$, and x_{3d} respectively converge to f_0, f_1, and x_3, then the error will also converge to a small ball o_s.

Now, we define a new state control error

$$e_3 = x_3 - x_{3d} \tag{21}$$

It follows that,

$$\dot{e}_3 = \frac{1}{f_4}(f_2 + f_3 + f_3 u) - \dot{x}_{3d} \tag{22}$$

For minimizing the new control error e_3 as the above analysis, the final control signal is synthesized as follows

$$u = -\frac{1}{\hat{f}_3}\left(\hat{f}_2 - \hat{f}_4 \dot{x}_{3d} + \frac{\beta_2}{\beta_3} s + k_3 \hat{f}_3 e_3 + e_{3s}\right) \tag{23}$$

where e_{3s} is a bounded function of e_3, while β_2, β_3 are positive constants and $k_3 > \Delta_{\dot{f}_4} / 2 f_{3\min}$.

The purpose of the functions s_s and e_{3s} is to improve the transient and steady-state performances of the control system, respectively. Thus, these functions are proposed as follows

$$\begin{cases} s_s = k_{2t}|s|s + k_{2s}\int_0^t s d\tau \\ e_{3s} = k_{3t}|e_3|e_3 + k_{3s}\int_0^t e_3 d\tau \end{cases} \tag{24}$$

where k_{2s}, k_{3s} are positive constants while the values of k_{2t}, k_{3t} are chosen as

$$\begin{cases} k_{2t} = \upsilon_2 \dfrac{k_2}{|s|_\infty} \\ k_{3t} = \upsilon_3 \dfrac{k_3 f_{3\min}}{|e_3|_\infty} \end{cases} \text{ where } \upsilon_{i|i\triangleq 2,3.} \in \left[0;\ \ 10^{-2}\right] \tag{25}$$

Because uncertainties exist in the designed rules, the control performance can be degraded in the case where large gaps occur between the real values and the used values. Hence, developing an estimation theory to identify the uncertain functions $f_{i|i\triangleq 0..4}$ as accurately as possible is critical here.

3.2 Model-based identification theory

Now, each function $f_{i|i\triangleq 0..4}$ can be divided into three parts as follows:

$$f_{i|i\triangleq 0..4.} \triangleq \Xi_i^T \Upsilon_i + \nu_i \tag{26}$$

which satisfy the following conditions

$$\begin{cases} |\nu_i| \ll |f_i|_{i\triangleq 0..4} \\ \Xi_i \in \Omega_i \triangleq \left[\Xi_{i\min};\ \ \Xi_{i\max}\right]_{i\triangleq 0..4.} \end{cases} \tag{27}$$

where Ω_i is feasible range of uncertain vector Ξ_i.

In order to estimate the uncertain parameters of the given system, an estimation system is proposed as

$$\begin{cases} \dot{\hat{x}}_2 = \dfrac{1}{\hat{f}_0}\left(x_3 + \hat{f}_1\right) - l_2 \tilde{x}_2 \\ \dot{\hat{x}}_3 = \dfrac{1}{\hat{f}_4}\left(\hat{f}_2 + \hat{f}_3 u\right) - l_3 \tilde{x}_3 \end{cases} \tag{28}$$

where

$$\hat{f}_{i|i\triangleq 0..4.} = \hat{\Xi}_i^T \Upsilon_i \tag{29}$$

and l_2, l_3 are positive constants.

From the given system Eq. (17) and the approximation system Eq. (28), the update laws of the uncertain parameters can be designed

$$\begin{cases} \dot{\hat{\Xi}}_0 = -\Gamma_{\hat{\Xi}_0}^{\Omega_0} R_{f_0}^{-1} \Upsilon_0 \alpha_2 e_{e2} \dot{\hat{x}}_2 \\ \dot{\hat{\Xi}}_1 = \Gamma_{\hat{\Xi}_1}^{\Omega_1} R_{f_1}^{-1} \Upsilon_1 \alpha_2 e_{e2} \\ \dot{\hat{\Xi}}_2 = \Gamma_{\hat{\Xi}_2}^{\Omega_2} R_{f_2}^{-1} \Upsilon_2 \alpha_3 e_{e3} \\ \dot{\hat{\Xi}}_3 = \Gamma_{\hat{\Xi}_3}^{\Omega_3} R_{f_3}^{-1} \Upsilon_3 \alpha_3 e_{e3} u \\ \dot{\hat{\Xi}}_4 = -\Gamma_{\hat{\Xi}_4}^{\Omega_4} R_{f_4}^{-1} \Upsilon_4 \alpha_3 e_{e3} \dot{\hat{x}}_3 \end{cases} \tag{30}$$

Here, $e_{ei|i\triangleq 2,3.} \triangleq -\tilde{x}_i = x_i - \hat{x}_i$. $R_{f_{i|i\triangleq 0..4.}}$ are positive-definite diagonal matrices and α_2, α_3 are positive constants. $\Gamma_{\hat{\Xi}_i}^{\Omega_i}|_{i\triangleq 0..4.}$ are diagonal matrices of boundary-guaranty functions which are simply designed as

$$\Gamma_{\hat{\Xi}_i}^{\Omega_i}(b, b_{\min}, b_{\max}, c)\Big|_{\substack{i\triangleq 0..4. \\ k\triangleq 1..length(\hat{\Xi}_i) \\ b\triangleq \hat{\Xi}_i(k) \\ b_{\min}\triangleq \Xi_{i\min}(k) \\ b_{\max}\triangleq \Xi_{i\max}(k) \\ \varepsilon_{ik}>0}} = \begin{cases} 1 - \dfrac{(b-b_{\min})(b-b_{\max})}{\varepsilon_{ik}(b_{\max}-b_{\min})^2} & \text{if}\left(cond\right) \\ 1 & \text{otherwise} \end{cases} \tag{31}$$

$$cond \triangleq \left(b \notin \left[b_{\min};\ \ b_{\max}\right]\right) \text{and} \left((2b - b_{\min} - b_{\max})c > 0\right)$$

To study the convergence of the proposed method, the following theorem is investigated,

Theorem 1:

Consider a nonlinear system as Eq. (17) satisfying *Assumptions 1* and *2*, and employ an estimation model (28) with the learning rules Eq. (30) under condition $l_3 > (\Delta_{\dot{f}_4} / (2 f_{4\min}))$. If the estimating vector errors are sufficiently rich, or $|\tilde{x}_2| > ((\Delta_{v_1} + \Delta_{\zeta_2})/l_2)$ and $|\tilde{x}_3| > 2(\Delta_{v_2} + \Delta_{v_3}\Delta_u + \Delta_{v_4}\Delta_{\dot{\hat{x}}_3} + \Delta_{\zeta_3})/(2 l_3 f_{4\min} - \Delta_{\dot{f}_4})$, in transient time, then the estimation model will converge to the system model with an allowable bound.

Proof:

Assumption 1.e indicates that function f_4 is always positive. Thus, consider a Lyapunov function as follows

$$V_1 = \frac{\alpha_2}{2} f_0 \tilde{x}_2^2 + \frac{\alpha_3}{2} f_4 \tilde{x}_3^2 + \frac{1}{2}\left(\sum_{i=0}^{4} \tilde{\Xi}_i^T R_{f_i} \tilde{\Xi}_i\right) \tag{32}$$

Differentiating the candidate function with respect to time and noting Eqs. (17) and (28) lead to

$$\begin{aligned} \dot{V}_1 &= \alpha_2 f_0 \tilde{x}_2 \dot{\tilde{x}}_2 + \frac{\alpha_3}{2} \dot{f}_4 \tilde{x}_3^2 + \alpha_3 f_4 \tilde{x}_3 \dot{\tilde{x}}_3 + \sum_{i=0}^{4} \tilde{\Xi}_i^T R_{f_i} \dot{\tilde{\Xi}}_i \\ &= \alpha_2 \tilde{x}_2 (-\tilde{f}_0 \dot{\hat{x}}_2 + \tilde{f}_1 - \nu_1 - \zeta_2 - l_2 \tilde{x}_2) + \frac{\alpha_3}{2} \dot{f}_4 \tilde{x}_3^2 + \sum_{i=0}^{4} \tilde{\Xi}_i^T R_{f_i} \dot{\tilde{\Xi}}_i \\ &+ \alpha_3 \tilde{x}_3 \left(-\tilde{f}_4 \dot{\hat{x}}_3 + \tilde{f}_2 + \tilde{f}_3 u - \nu_2 - \nu_3 u + \nu_4 \dot{\hat{x}}_3 - \zeta_3 - l_3 \hat{f}_4 \tilde{x}_3\right) \end{aligned} \tag{33}$$

Employing the learning laws (Eq. (30)) yields

$$\begin{aligned}\dot{V}_1 &= \alpha_2\tilde{x}_2(-\tilde{\Xi}_0^T\Upsilon_0\dot{\hat{x}}_2+\tilde{\Xi}_1^T\Upsilon_1-v_1-\zeta_2-l_2\tilde{x}_2)\\ &+\frac{\alpha_3}{2}\dot{f}_4\tilde{x}_3^2+\sum_{i=0}^{4}\tilde{\Xi}_i^T R_{f_i}\dot{\tilde{\Xi}}_i+\alpha_3\tilde{x}_3\left(-\tilde{\Xi}_4^T\Upsilon_4\dot{\hat{x}}_3+\tilde{\Xi}_2^T\Upsilon_2\right)\\ &+\alpha_3\tilde{x}_3\left(\tilde{\Xi}_3^T\Upsilon_3 u-v_2-v_3u+v_4\dot{\hat{x}}_3-\zeta_3-l_3\hat{f}_4\tilde{x}_3\right)\\ &\le-\alpha_2\tilde{x}_2(v_1+\zeta_2+l_2\tilde{x}_2)\\ &-\alpha_3\tilde{x}_3\left(v_2+v_3u-v_4\dot{\hat{x}}_3+\zeta_3+\left(l_3\hat{f}_4-\frac{1}{2}\dot{f}_4\right)\tilde{x}_3\right)\end{aligned} \tag{34}$$

Here, *Theorem 1* is proven.

Remark 2:

The convergence of the identification method strongly depends on boundaries of the unknown terms and the working range of the system. The magnitude of the unknown boundaries is significantly reduced by obtaining an accurate mathematical model of the studied system as in Section 2. Moreover, to increase the convergence rate of the method, the value of l_2, l_3 and time derivative of the state variable should be sufficiently large.

The final goal of the paper is to supply a precise controller for the tracking control. A good identification result presents the good adaptation of the proposed approach with the system change and leads to the use of the smaller robust gains in the control signals, while a proper control strategy could provide excellent performance with less control effort. However, in the real-time applications, the update laws can be degraded in the case of simple trajectories.

3.3 Integrated mechanism

To increase the excitation ability of the identification process, the estimation method is integrated into the robust nonlinear controller. Here, the learning laws (Eq. (30)) are improved by adding some excitation terms as follows

$$\begin{cases}\dot{\hat{\Xi}}_0=-\Gamma_{\hat{\Xi}_0}^{\Omega_0}R_{f_0}^{-1}\Upsilon_0\left(\alpha_2 e_{e2}\dot{\hat{x}}_2+\beta_2 s\left(\ddot{x}_d-k_1\dot{e}\right)\right)\\ \dot{\hat{\Xi}}_1=\Gamma_{\hat{\Xi}_1}^{\Omega_1}R_{f_1}^{-1}\Upsilon_1(\alpha_2 e_{e2}+\beta_2 s)\\ \dot{\hat{\Xi}}_2=\Gamma_{\hat{\Xi}_2}^{\Omega_2}R_{f_2}^{-1}\Upsilon_2(\alpha_3 e_{e3}+\beta_3 e_3)\\ \dot{\hat{\Xi}}_3=\Gamma_{\hat{\Xi}_3}^{\Omega_3}R_{f_3}^{-1}\Upsilon_3 u(\alpha_3 e_{e3}+\beta_3 e_3)\\ \dot{\hat{\Xi}}_4=-\Gamma_{\hat{\Xi}_4}^{\Omega_4}R_{f_4}^{-1}\Upsilon_4(\alpha_3 e_{e3}\dot{\hat{x}}_3+\beta_3 e_3\dot{x}_{3d})\end{cases} \tag{35}$$

To verify the convergence of the closed-loop system, a new theorem is studied.

Theorem 2:

Given a bounded nonlinear system Eq. (12) under *Assumptions* 2 and *3*, employing the control laws Eq. (18)~(25) incorporated with the identification mechanism Eq. (28)~(31) and the improvement Eq. (35), the following properties hold:

If the estimation errors and the state control errors are sufficiently rich in transient time or $|\tilde{x}_2|>((\Delta_{v_1}+\Delta_{\zeta_2})/l_2)$, $|\tilde{x}_3|>2(\Delta_{v_2}+\Delta_{v_3}\Delta_u+\Delta_{\dot{x}_3}+\Delta_{\zeta_3})/(2l_3 f_{4\min}-\Delta_{\dot{f}_4})$, $|s|>(\mho_{v_1+\xi_2}/k_2)$, and $|e_3|>(2\mho_{v_2+v_3u-v_4\dot{x}_{3d}+\zeta_3}/2k_3 f_{3\min}-\Delta_{\dot{f}_4})$, the uncertain parameters of the system will then converge to the real values with an allowable bound.

By properly selecting the control parameters k_1 and k_i, k_{it}, $k_{is}\,|_{i\triangleq 2,3.}$, the tracking control error of the closed-loop system will converge to a desired bound via the strict convergence of the other state control errors.

Proof:

Define some unknown bounded terms as follows

$$\begin{cases}\xi_2\triangleq\zeta_2+v_1\in\left[p_2-\frac{\mho_{\xi_2}}{2};\quad p_2+\frac{\mho_{\xi_2}}{2}\right]\\ \xi_3\triangleq\zeta_3+v_2+v_3u-v_4\dot{x}_{3d}\in\left[p_3-\frac{\mho_{\xi_3}}{2};\quad p_3+\frac{\mho_{\xi_3}}{2}\right]\end{cases} \tag{36}$$

where $p_{i|i\triangleq 2,3}$ are the center points of the feasible ranges of $\xi_{i|i\triangleq 2,3.}$.

The unknown terms can be re-expressed as

$$\xi_{i|i\triangleq 2,3.}\triangleq p_i+\vartheta_i,\ \text{where}\ \vartheta_i\in\left[-\mho_{\xi_i};\quad\mho_{\xi_i}\right] \tag{37}$$

Consider a new composited Lyapunov function as

$$\begin{aligned}V_2 &= V_1+\frac{1}{2}\beta_2 f_0 s^2+\frac{1}{2}\beta_3 f_4 e_3^2\\ &+\frac{\beta_2}{2k_{2s}}(k_{2s}s-p_2)^2+\frac{\beta_3}{2k_{3s}}(k_{3s}e_{3s}-p_3)^2\end{aligned} \tag{38}$$

Applying the control laws Eqs. (18)~(25), the time derivative of the function V_2 becomes

$$\begin{aligned}\dot{V}_2 &= \dot{V}_1-(k_2\beta_2 s^2+\beta_2 s(k_{2t}|s|s-\vartheta_2))\\ &-\left(k_3\beta_3\hat{f}_3 e_3^2+\beta_3 e_3\left(k_{3t}|e_3|e_3-\vartheta_3-\frac{1}{2}\dot{f}_4 e_3\right)\right)\\ &-\beta_2 s(\tilde{f}_1-\tilde{f}_0(\ddot{x}_d-k_1\dot{e}))-\beta_3 e_3(\tilde{f}_2+\tilde{f}_3 u-\tilde{f}_4\dot{x}_{3d})\end{aligned} \tag{39}$$

Noting the improvement Eq. (35) and the result of *Theorem 1* yields

$$\begin{aligned}\dot{V}_2 &\le-\beta_2 s\left(\left(k_2+k_{2t}\,|s|\right)s-\vartheta_2\right)-\alpha_2\tilde{x}_2(v_1+\zeta_2+l_2\tilde{x}_2)\\ &-\beta_3 e_3\left(\left(k_3\hat{f}_3+k_{3t}\,|e_3|-\frac{1}{2}\dot{f}_4\right)e_3-\vartheta_3\right)\\ &-\alpha_3\tilde{x}_3\left(v_2+v_3u-v_4\dot{\hat{x}}_3+\zeta_3+(l_3\hat{f}_4-\frac{\dot{f}_4}{2})\tilde{x}_3\right)\end{aligned} \tag{40}$$

Here, the first statement of *Theorem 2* has been proven.

From the above inequality, the following bound is determined

$$|e_3|_\infty\le\sqrt{\gamma}+\frac{\Delta_{\vartheta_3}}{2\breve{k}_3} \tag{41}$$

where $\breve{k}_3=k_3\hat{f}_{3\min}-\frac{1}{2}\Delta_{\dot{f}_4}$ and

$$\begin{aligned}\gamma &= \frac{\Delta_{\vartheta_3}^2}{4\breve{k}_3^2}+\frac{1}{\beta_3\breve{k}_3}\frac{\beta_2\Delta_{\vartheta_2}^2}{4k_2}\\ &+\frac{1}{\beta_3\breve{k}_3}\alpha_2\Delta_{\xi_2}\min\left(|\tilde{x}_2|,\frac{\Delta_{\xi_2}}{4l_2}\right)\\ &+\frac{1}{\beta_3\breve{k}_3}\alpha_3\Delta_{\xi_3}\min\left(|\tilde{x}_3|,\frac{\Delta_{\xi_3}}{4\left(l_3\hat{f}_{4\min}-\frac{1}{2}\Delta_{\dot{f}_4}\right)}\right)\end{aligned}$$

When only applying these control rules to the force dynamics, the following relationship is given

$$|s|_\infty\le\sqrt{\frac{\left|e_{3\infty}+\vartheta_2\right|^2}{4k_2^2}+\frac{1}{\beta_2 k_2}\alpha_2|\xi_2|\min\left(|\tilde{x}_2|,\frac{|\xi_2|}{4l_2}\right)}+\frac{|e_{3\infty}+\vartheta_2|}{2k_2} \tag{42}$$

Because the state control signal x_{3d} is used to compensate for the

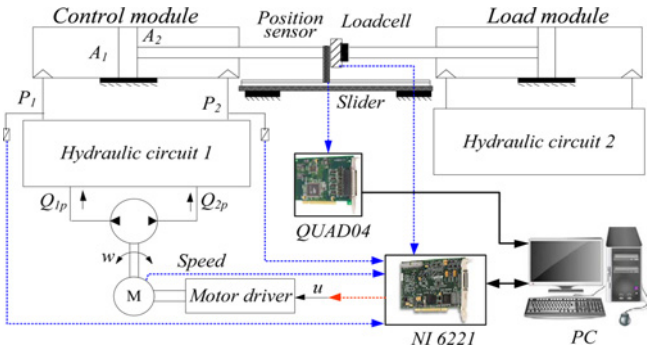

Fig. 2 Experimental configuration

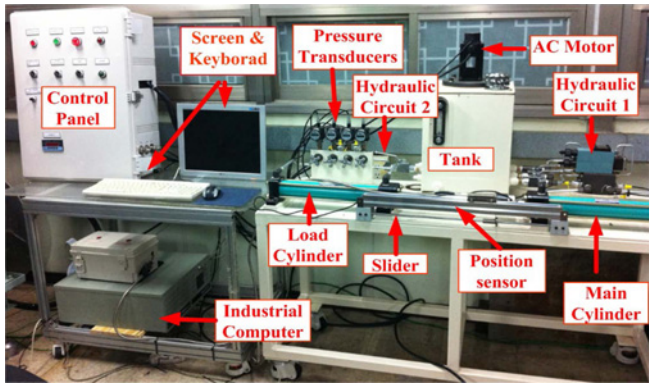

Fig. 3 Photograph of the experimental apparatus

unknown term ζ_2, IEQ. (42) becomes

$$|s|_\infty \to \sqrt{\frac{(|e_3|_\infty - \Delta_{g_2})^2}{4k_2^2} + \frac{1}{4}\alpha_2 \Delta_{\xi_2} \min\left(|\tilde{x}_2|, \frac{\Delta_{\xi_1}}{4l_2}\right)} + \frac{|e_3|_\infty - \Delta_{g_2}|}{2k_2} \quad (43)$$

A combination of Eqs. (18), (41) and (43) leads to the proof of the second statement of *Theorem 2*.

Remark 3:

In this section, the influence of the identification mechanism on the control performance has been clearly derived. Some poor identification results could increase the control error. The effectiveness of the state control theory has also been addressed. In order to easily apply the proposed approach to real-time applications, the implementation procedures of the estimation theory and the integrated controller are summarized in Appendix A and Appendix B, respectively.

4. Experimental Validation

In this section, the performance of the proposed approach has been verified through real-time experiments. For this purpose, an experimental system was built as depicted in Fig. 2. This system consisted of the studied hydraulic circuit as introduced in Section 2 (Fig. 1), and a control-data acquisition (CDAQ) system. The CDAQ system included an Advantech Industrial Computer (Core i3-2100 3.1 GHz), a data acquisition (DAQ) card (PCI-6221), an encoder reader (PCI-QUAD 04), and proper sensors. The displacement of the actuator and the working pressures were measured using a linear encoder (WTB5-500 MM) and pressure transducers (DS-230), respectively. The external force was validated via a load-cell (YC60-2T) and an indicator. The designed controller was implemented on the computer within Real-time Window Target Toolbox of Matlab under a sampling time of 2 ms. The detailed specifications of the system components are summarized in Table 1, while the real apparatus is displayed in Fig. 3.

To validate the identification method according to the procedure described in Appendix A, a random signal – plotted in Fig. 4 – was selected as the system input for an open-loop experiment. The purpose of this experiment was to determine the believable values of the uncertain parameters. Detailed structures of the uncertain terms extracted from the functions $f_{i|i\triangleq 0..4}$ can be seen in Appendix C. The other system parameters and the range of the uncertain parameters were set as in Tables 2 and 3, respectively. The estimation rate matrices and error gains were then chosen as follows:

$$\alpha_2 = 2.5\times10^{-4}; \quad \alpha_3 = 2.05\times10^{6}; \quad R_{f_0}^{-1} = 650;$$

$$R_{f_1}^{-1} = diag([225\times10^{4}; 2.57\times10^{8}; 3.02\times10^{9}]);$$

$$R_{f_2}^{-1} = diag(49\times10^{-6}; 53\times10^{-6}; 3.9\times10^{-16}; 4.03\times10^{-18});$$

$$R_{f_3}^{-1} = 4.6\times10^{-10}; \quad R_{f_4}^{-1} = 2.48\times10^{-10}; \quad l_2 = 261; \quad l_3 = 140.$$

Table 1 Specifications of the studied system

Device	Specification
Hydraulic cylinder	Type: DAJON D140H-SD50B-N300
	Stroke: 300 [mm]
	Tube diameter: 50 [mm]
	Rod diameter: 30 [mm]
Hydraulic pump	Type: GALTECH 2SM-G-4-R-SAEA-13GGA-VT
	Displacement: 4 [cc/rev]
	Max. speed: 4000 [rpm]
	Max. flow: 16 [lt/min]
AC Servo motor	Type: HIGEN FMACN10-AB00
	Power: 1 [kW]
	Max. speed: 3000 [rpm]
Motor driver	Type: HIGEN FDA7010
	Max. current: 6.9 [A]
	Power: 1 [kW]

Table 2 The system parameters obtained from the manufactures

Parameter	Nomen	Value
Stroke length	d_t (m)	0.3
Bore area	A_1 (m^2)	1.9635×10^{-3}
Rod area	A_2 (m^2)	1.2566×10^{-3}
Pump displacement	D (m^3/rev)	4×10^{-6}
Driver gain	K_{dr} (rev/(*Vs*))	5

Table 3 Chosen ranges of uncertain vectors

Uncertain Vector	Max Value	Min Value
Ξ_0	50	0.8
Ξ_1	$[100 \quad 3000 \quad 700]^T$	$[2 \quad 10 \quad 50]^T$
Ξ_2	$[4.9\times10^{-4} \quad 4.2\times10^{-4}$ $1.6\times10^{-10} \quad 1.2\times10^{-15}]^T$	$[3.1\times10^{-4} \quad 2.2\times10^{-4}$ $5\times10^{-11} \quad 3\times10^{-18}]^T$
Ξ_3	5.5×10^{-5}	10^{-7}
Ξ_4	2×10^{-8}	6.67×10^{-10}

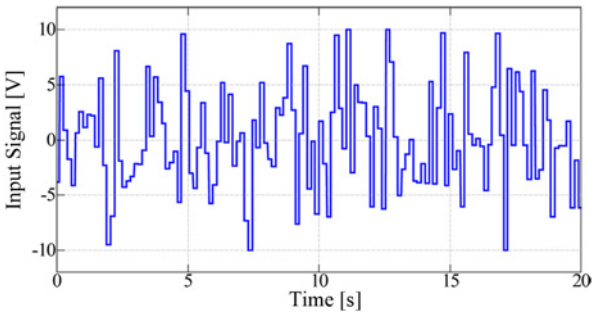

Fig. 4 Random input signal for open-loop experiment

The initial values of the uncertain parameters were randomly set within their possible ranges. This random selection could lead to differences between the estimated values (Eq. (28)) and the measured values of the velocity and pressure at the beginning. However, by applying the learning mechanism (Eq. (30)), all the parameters were stabilized at the steady-state values and the estimation errors were converged to remarkable ranges. As seen in Figs. 5 and 7, the estimation error of the velocity reduced from ([-0.16; 0.07] (m/s)) to (±0.0065 (m/s)) while that of the pressure was from ([-250; 320] (N)) to (±40 N). From Figs. 6 and 8, the believable values of the parameters were also easily determined:

$$M = 9.32(kg), b_1 = 6.6(N/m), b_{23} = 258(Ns/m), b_4 = 532(N)$$

$$V_{10} = 4.375\times10^{-4}; V_{20} = 2.88\times10^{-4}; C_{cLi} = 1.51\times10^{-10};$$

$$C_{cPi1} \triangleq \frac{4\pi^2}{\eta_v D} C_{pLi} J_{HP} = 2.4\times10^{-16}; \beta_e = 5.34\times10^{8};$$

$$D_1 \triangleq (\eta_v D + T_{fHP}\frac{4\pi^2 C_{cLi}}{\eta_v D}) = 5.83\times10^{-7}.$$

Although the real values of the uncertain parameters were unknown, the convergence of the estimation process of both the parameters and the estimation errors demonstrated the effectiveness of the algorithm. The feasible ranges of the parameters were reconfigured more certainly.

Next, the controller derived in Section 3 was implemented on the testing system for position-tracking control following the procedure described in Appendix B. Chirp, sinusoidal, and smooth multi-step signals were chosen as the desired trajectories to evaluate the controller. The results obtained in the open-loop experiment were used as the initial values of the control parameters. Other parameters were finally selected as follows:

$$k_1 = 352; \quad k_2 = 490; \quad k_{2s} = 15;$$
$$k_{2t} = 0.12; \quad \beta_2 = 2.2\times10^{-4}; \quad k_3 = 0.21;$$
$$k_{3s} = 2.1\times10^{-2}; \quad k_{3t} = 0.5\times10^{-23}; \quad \beta_3 = 2.1\times10^{5}.$$

Additionally, a tuned PID controller[25] and a direct backstepping (DBS) controller were employed for comparison of the proposed controller on the same system under the same testing conditions. The DBS controller was designed the same as that made by Ahn et al.[19] while the PID gains were tuned to be K_P=551.12, K_I=6.15, K_D=0.203.

In the first experimental case, a chirp signal with amplitude of 100 mm and maximum frequency of 0.1 Hz, as shown in Fig. 9, was chosen as the reference input of the closed-loop system. By applying the PID, the DBS and the designed controllers to the system, the tracking errors were compared as presented in Fig. 10. From the information of the control error, the PID controller produced an appropriate control signal to force the error to be as small as possible. As seen in the figure, a good range of the control error was clearly obtained ([0.97→1.73] (mm) ~ [0.97%→1.73%]) by using this controller. On the other hand, to

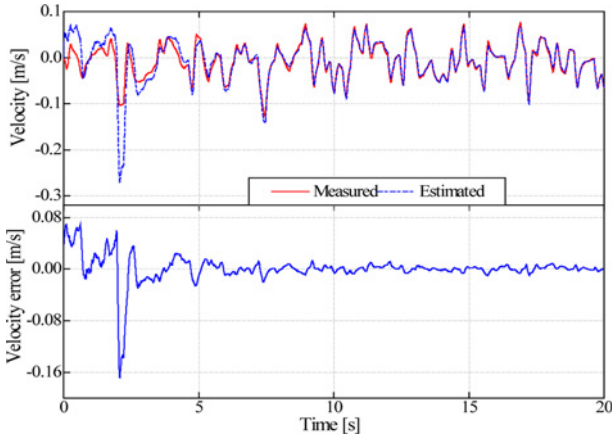

Fig. 5 Identification results of the force dynamics from open-loop experiment

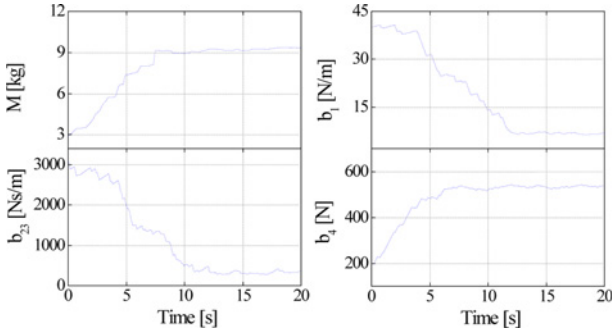

Fig. 6 Estimated parameters of the force dynamics

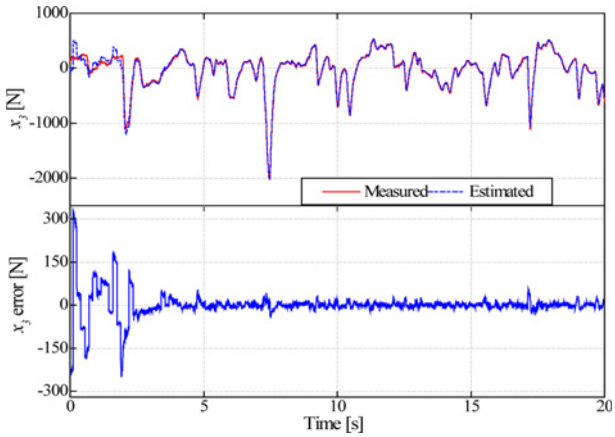

Fig. 7 Identification results of the pressure dynamics from open-loop experiment

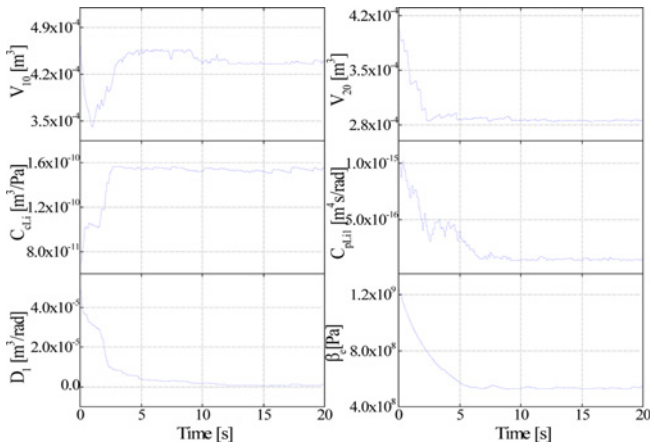

Fig. 8 Estimated parameters of the pressure dynamics

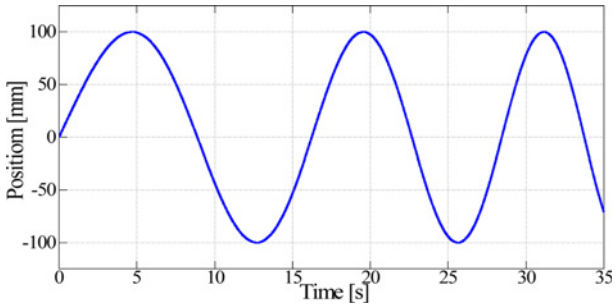

Fig. 9 Reference input signal of the first experimental case

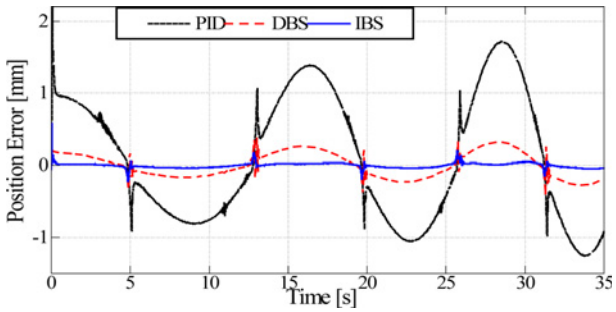

Fig. 10 Comparative control errors in the first experimental case

improve the control performance, the DBS controller employed adaptive nonlinear terms to compensate for the system nonlinearities, and robust gains to minimize the control error. Thus, a better range of the control error was given ([0.22→0.45] (mm) ~ [0.22%→0.45%]). However, it can be seen that the control performance worsened when the working frequency increased. This drawback is due to the incomprehensive system modeling and the learning mechanism of the uncertain parameters. In the DBS design,[19] some nonlinear functions were only considered as uncertain parameters, while it was not certain whether the initial values of the uncertain parameters were chosen close to the real values in the control process. These issues have been addressed in the proposed approach by the fully mathematical system model and the

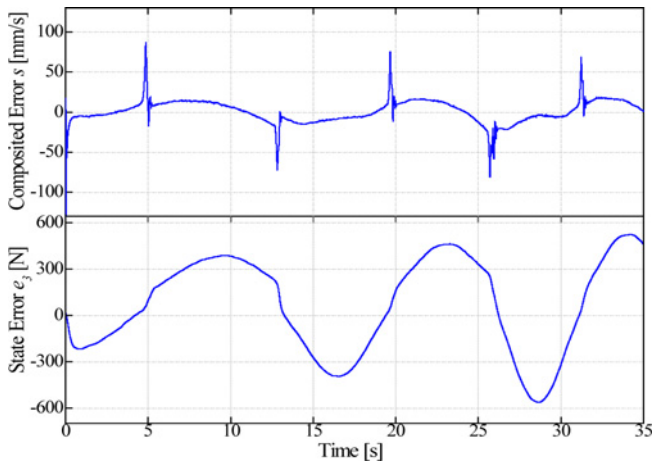

Fig. 11 State errors of the proposed controller in the first experimental case

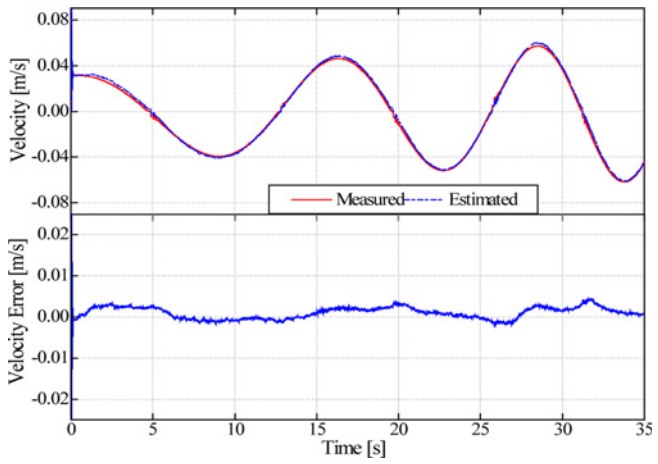

Fig. 12 Identification results of the force dynamics in the first experimental case

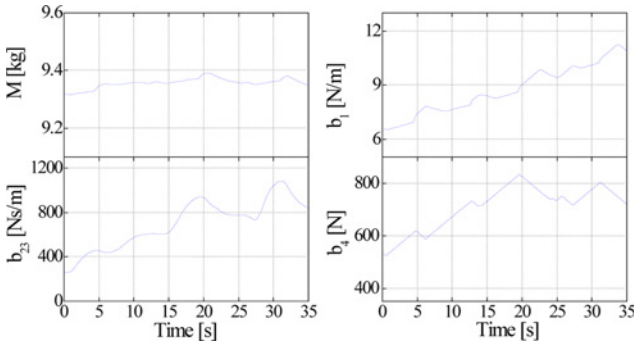

Fig. 13 Estimated parameters of the force dynamics in the first experimental case

novel online identification method. Moreover, some advanced functions of the state control errors are adopted inside the control signal to enhance the transient and steady-state control performances. As a result,

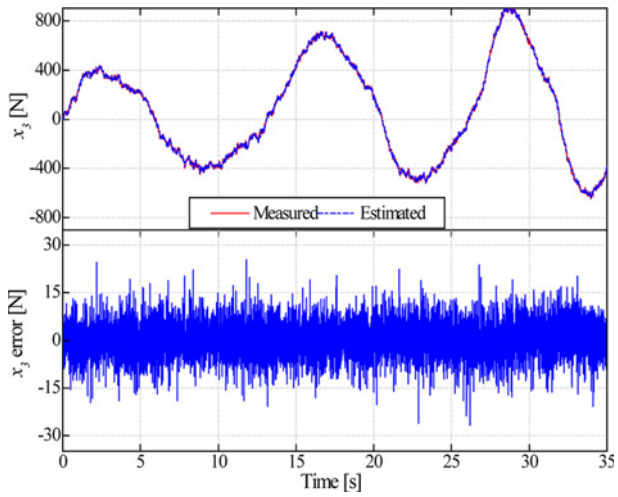

Fig. 14 Identification results of the pressure dynamics in the first experimental case

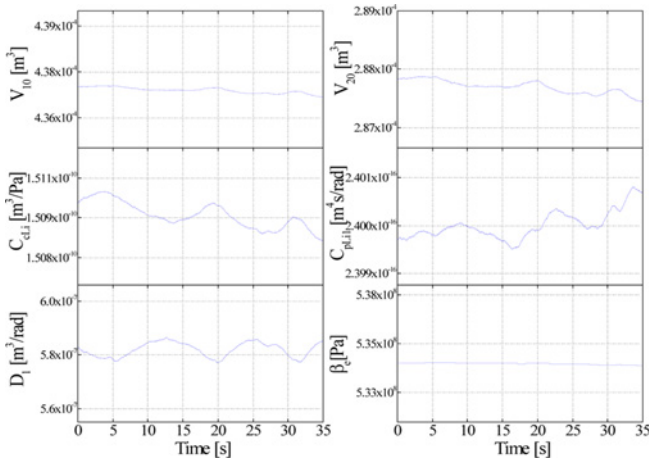

Fig. 15 Estimated parameters of the pressure dynamics in the first experimental case

an excellent control error was achieved (±0.04 mm ~ 0.04%). Other state control errors are illustrated in Fig. 11, while the online-running estimation results are also displayed in Figs. 12 to 15. Combining with Fig. 16, these figures show that, in spite of the increase in the external force, the estimation error of the force dynamic was still maintained in an acceptable range. The control and estimation results remark that the integrated control algorithm could adapt well with both the changes of the system and the external disturbance. Besides, the smooth form of the control input, as plotted in Fig. 17, demonstrates the feasibility of the control method. Hence, the effectiveness of the proposed method has been confirmed. Nevertheless, peak points occurred when the system direction changed. This phenomenon is explained by the presence of the system hysteresis which is not studied in this article (*Assumption 1.g*).

In the second experiment, for the more difficult challenge of the proposed approach in the tracking control, a sinusoidal signal with a frequency of 0.5 Hz and amplitude of 20 mm was chosen as the reference input. After applying the same controllers as those in the first

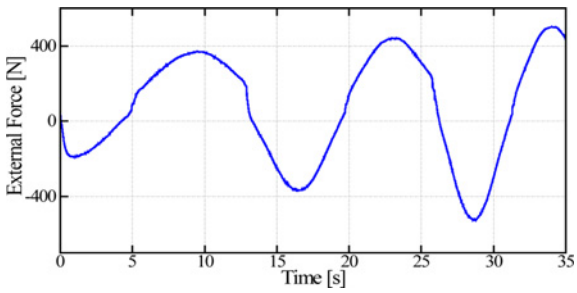

Fig. 16 External force in the first experimental case

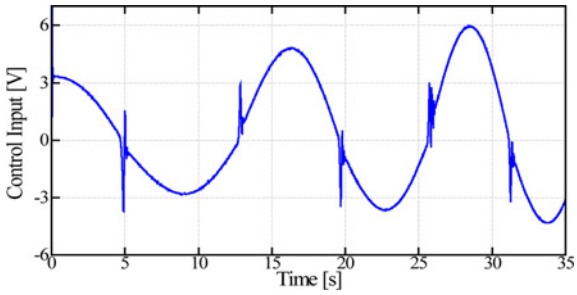

Fig. 17 Control input signal of the proposed controller in the first experimental case

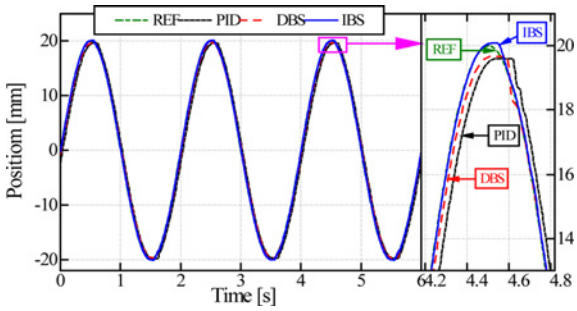

Fig. 18 Comparative responses of the second experiment

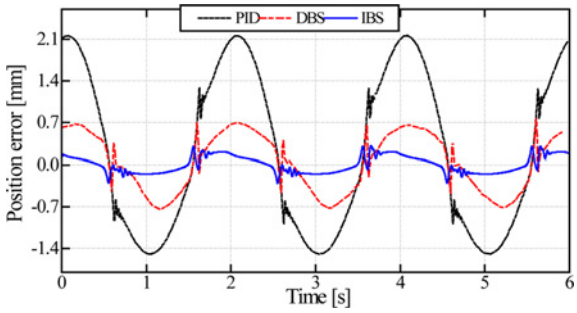

Fig. 19 Comparative control errors of the second experiment

experiment, the responses and the control errors of three of the methods were compared as described in Figs. 18~19. In this case, the control errors of the PID and DBS controllers were distinctly increased to new

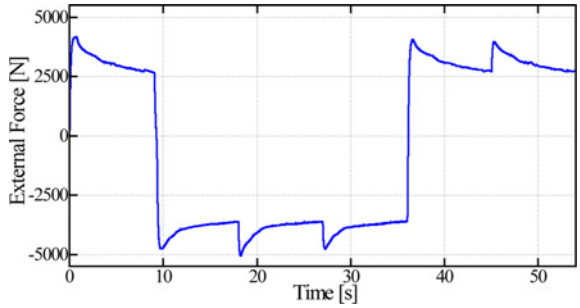

Fig. 20 External force in the last experiment

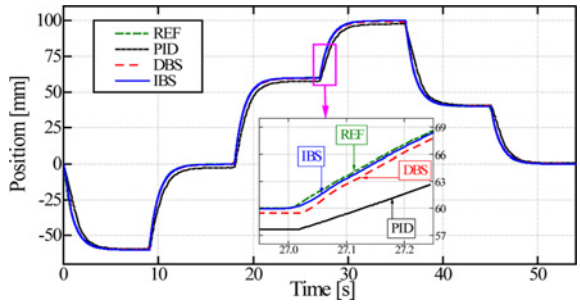

Fig. 21 Comparative responses in the last experiment

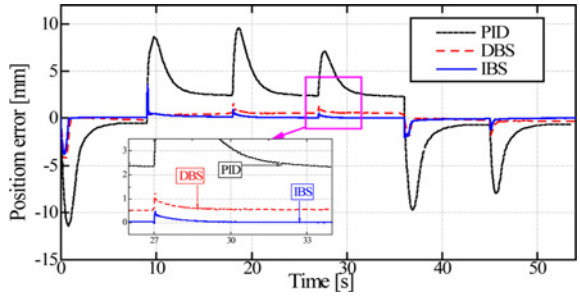

Fig. 22 Comparative control errors in the last experiment

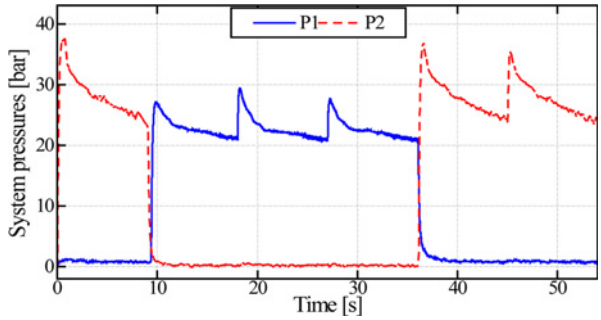

Fig. 23 Working pressures in the last experiment

ranges of [-1.5~2.22] (mm) (~11.1%) and [-0.7~0.69] (mm) (~3.5%), respectively. Meanwhile, through employing the improvement points, the performance of the proposed controller was still in the expected range (±0.3 mm (~1.5%) of control error). The tracking performance of the studied controller at a higher frequency is thus more definitely confirmed.

In the last experiment, to further investigate the transient response, the steady-state behavior, and the loading effect of the proposed approach, a smooth multi-step signal with maximum amplitude of 100 mm was used as the reference input while the external force was varied as shown in Fig. 20 by regulating the limited pressures of the relief valves in the load module. By employing the same controllers in the system as those used in the previous cases, the position responses and control errors were obtained as shown in Figs. 21 and 22. As seen in these figures, it was difficult to maintain a good result for the PID controller in both transient behavior (6.2 s of transient time) and steady-state response (2.35 mm (~2.35%) of the steady-state control error) under the heavy load condition. By possessing the robust gains and the state control strategy, the performance of the DBS method was remarkably improved compared to the PID controller. In detail, the transient time and steady-state control error were reduced to 3 s and 0.5 mm (~0.5%), respectively. Meanwhile, because the improvement for both transient and steady-state behaviors was employed in the proposed control approach, the tracking error was then converged to 0.015 mm (~0.015%) within about 2 s, regardless of the hard load variation. The working pressures are presented in Fig. 23. The figure demonstrates that the system efficiency has significantly increased. When the system operated, only the appropriate pressure was changed. Another pressure, which hindered the system movement, was negative or almost zero. This means that the drawback of the valve-controlled system has been resolved by the pump-controlled system. Here, the effectiveness of the proposed control in the transient, steady-state response, and load effect was strongly confirmed via this experiment.

5. Conclusions

In this article, the advanced controller incorporated with the novel identification method was introduced to control a pump-controlled hydraulic system. The mathematical model of the studied system, identification theory, and proposed control algorithm with improvements were comprehensively derived. The stability of both the identification approach and the closed-loop system was guaranteed through Lyapunov functions.

The feasibility and effectiveness of the designed controller were then successfully verified by comparing with the tuned PID controller and the direct backstepping controller in the real-time position-tracking of the PEHS test-bed under many working conditions. The results convincingly demonstrate the adaptation and robustness of the proposed method over the compared methods.

However, this research has some limitations. The influence of deploying the continuous-time (identification and control) theories on the discrete-time domain was not studied. Moreover, the experimental results showed that the control performance worsened as the system changed direction. Thus, some extensive studies of these problems are considered as future works of this paper.

ACKNOWLEDGEMENT

This work was supported by the Human Resource Training Program for Regional Innovation and Creativity through the Ministry of Education and National Research Foundation of Korea (NRF-2015H1C1A1035547) and by the Technology Innovation Program (10043810, Development of a 20~40kW smart hybrid powerpack for industry based on intelligent control) funded By the Ministry of Trade, Industry & Energy (MI, Korea).

REFERENCES

1. Kawasaki Heavy Industries, Ltd., "Hydraulic Systems for Industrial Use," http://global.kawasaki.com/en/industrial_equipment/hydraulic/pdf/sanki_JE_150427a.pdf (Accessed 13 APR 2016)
2. Volvo, "Volvo Excavators EC380E," http://www.volvoce.com/SiteCollectionDocuments/VCE/Documents%20North%20America/crawler%20excavators/Volvo_EC380EProductBrochure%203-14-14.pdf (Accessed 17 MAR 2016)
3. Sany Group Co., Ltd., "Truck Cranes: QY100," http://www.sanygroup.com/products/en-us/hoisting/QY100.htm (Accessed 17 MAR 2016)
4. Alleyne, A. and Hedrick, J. K., "Nonlinear Adaptive Control of Active Suspensions," IEEE Transactions on Control Systems Technology, Vol. 3, No. 1, pp. 94-101, 1995.
5. Yao, B., Bu, F., Reedy, J., and Chiu, G. T., "Adaptive Robust Motion Control of Single-Rod Hydraulic Actuators: Theory and Experiments," IEEE/ASME Transactions on Mechatronics, Vol. 5, No. 1, pp. 79-91, 2000.
6. Habibi, S. and Goldenberg, A., "Design of a New High Performance Electrohydraulic Actuator," Proc. of IEEE/ASME International Conference on Advanced Intelligent Mechatronics, pp. 227-232, 1999.
7. Grabbel, J. and Ivantysynova, M., "An Investigation of Swash Plate Control Concepts for Displacement Controlled Actuators," International Journal of Fluid Power, Vol. 6, No. 2, pp. 19-36, 2005.
8. Aly, A. A., "PID Parameters Optimization using Genetic Algorithm Technique for Electrohydraulic Servo Control System," Intelligent Control and Automation, Vol. 2, No. 2, pp. 69-76, 2011.
9. Truong, D. Q. and Ahn, K. K., "Force Control for Press Machines using an Online Smart Tuning Fuzzy PID based on a Robust Extended Kalman Filter," Expert Systems with Applications, Vol. 38, No. 5, pp. 5879-5894, 2011.
10. Zhao, J., Wang, J., and Wang, S., "Fractional Order Control to the Electro-Hydraulic System in Insulator Fatigue Test Device," Mechatronics, Vol. 23, No. 7, pp. 828-839, 2013.
11. Tsao, T.-C. and Tomizuka, M., "Robust Adaptive and Repetitive Digital Tracking Control and Application to a Hydraulic Servo for Noncircular Machining," Journal of Dynamic Systems, Measurement, and Control, Vol. 116, No. 1, pp. 24-32, 1994.
12. Plummer, A. R. and Vaughan, N., "Robust Adaptive Control for Hydraulic Servosystems," Journal of Dynamic Systems, Measurement, and Control, Vol. 118, No. 2, pp. 237-244, 1996.
13. Bobrow, J. E. and Lum, K., "Adaptive, High Bandwidth Control of a Hydraulic Actuator," Journal of Dynamic Systems, Measurement, And Control, Vol. 118, No. 4, pp. 714-720, 1996.
14. Vossoughi, G. and Donath, M., "Dynamic Feedback Linearization for Electrohydraulically Actuated Control Systems," Journal of Dynamic Systems, Measurement, And Control, Vol. 117, No. 4, pp. 468-477, 1995.
15. Re, L. D. and Isidori, A., "Performance Enhancement of Nonlinear Drives by Feedback Linearization of Linear-Bilinear Cascade Models," IEEE Transactions on Control Systems Technology, Vol. 3, No. 3, pp. 299-308, 1995.
16. Yu, W.-S. and Kuo, T.-S., "Continuous-Time Indirect Adaptive Control of the Electrohydraulic Servo Systems," IEEE Transactions on Control Systems Technology, Vol. 5, No. 2, pp. 163-177, 1997.
17. Merritt, H. E., "Hydraulic Control Systems," John Wiley & Sons, 1967.
18. Lin, Y., Shi, Y., and Burton, R., "Modeling and Robust Discrete-Time Sliding-Mode Control Design for a Fluid Power Electrohydraulic Actuator (EHA) System," IEEE/ASME Transactions on Mechatronics, Vol. 18, No. 1, pp. 1-10, 2013.
19. Ahn, K. K., Nam, D. N. C., and Jin, M., "Adaptive Backstepping Control of an Electrohydraulic Actuator," IEEE/ASME Transactions on Mechatronics, Vol. 19, No. 3, pp. 987-995, 2014.
20. Tri, N. M., Nam, D. N. C., Park, H. G., and Ahn, K. K., "Trajectory Control of an Electro Hydraulic Actuator using an Iterative Backstepping Control Scheme," Mechatronics, Vol. 29, pp. 96-102, 2015.
21. Kaddissi, C., Kenné, J.-P., and Saad, M., "Identification and Real-Time Control of an Electrohydraulic Servo System based on Nonlinear Backstepping," IEEE/ASME Transactions on Mechatronics, Vol. 12, No. 1, pp. 12-22, 2007.
22. Mohanty, A. and Yao, B., "Integrated Direct/Indirect Adaptive Robust Control of Hydraulic Manipulators with Valve Deadband," IEEE/ASME Transactions on Mechatronics, Vol. 16, No. 4, pp. 707-715, 2011.
23. Mohanty, A. and Yao, B., "Indirect Adaptive Robust Control of Hydraulic Manipulators with Accurate Parameter Estimates," IEEE Transactions on Control Systems Technology, Vol. 19, No. 3, pp. 567-575, 2011.
24. Wang, L., Book, W. J., and Huggins, J. D., "Application of Singular Perturbation Theory to Hydraulic Pump Controlled Systems," IEEE/ASME Transactions on Mechatronics, Vol. 17, No. 2, pp. 251-259, 2012.
25. Thanh, T. D. C. and Ahn, K. K., "Nonlinear PID Control to Improve

the Control Performance of 2 Axes Pneumatic Artificial Muscle Manipulator using Neural Network," Mechatronics, Vol. 16, No. 9, pp. 577-587, 2006.

26. Jelali, M. and Kroll, A., "Hydraulic Servo-Systems: Modelling, Identification and Control," Springer Science & Business Media, 2012.

27. Manring, N., "Hydraulic Control Systems," Wiley, p. 111, 2005.

APPENDIX A

Procedure to implement the estimation theory in Subsection 3.2 is briefly described as shown in Fig. 24.

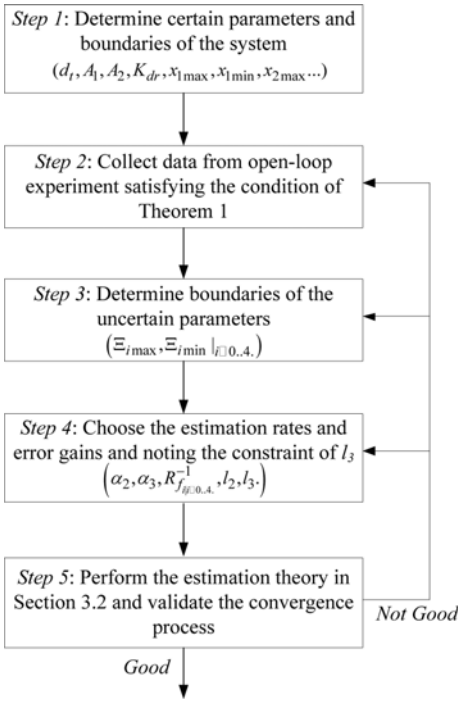

Fig. 24 Implementation procedure of the proposed estimation method

APPENDIX B

Procedure to perform the integrated controller in Subsections 3.1 and 3.3 is summarized as shown in Fig. 25.

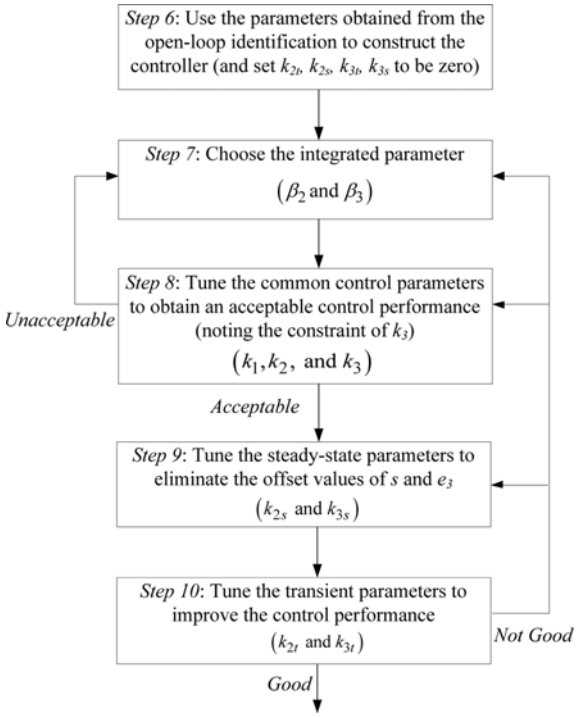

Fig. 25 Implementation Procedure of the proposed controller

APPENDIX C

The certain, uncertain and unknown terms extracted from the uncertain functions $f_{i|i\triangleq 0..4.}$ are specifically presented as follows:

$$f_0 \Rightarrow \begin{cases} \gamma_0 = 1 \\ \Xi_0 = M \\ \nu_0 = 0 \end{cases} \tag{44}$$

$$f_1 \Rightarrow \begin{cases} \gamma_1 = -[x_1 \quad x_2 \quad \tanh(x_2)]^T \\ \Xi_1 = [b_1 \quad (b_2 + b_3) \quad b_4]^T = [b_1 \quad b_{23} \quad b_4]^T \\ \nu_1 = 0 \end{cases} \tag{45}$$

$$f_2 \Rightarrow \begin{cases} \Upsilon_2 = \left[\Upsilon_{21} \quad \Upsilon_{22} \quad \Upsilon_{23} \quad \Upsilon_{24}\right]^T \\ \quad \Upsilon_{21} \triangleq -x_2\left(A_2^2 + A_2(A_1 - A_2)sm(x_2)\right) \\ \quad \Upsilon_{22} \triangleq -x_2\left(A_1^2 - A_1(A_1 - A_2)sm(-x_2)\right) \\ \quad \Upsilon_{23} \triangleq -(V_{20}A_1 + V_{10}A_2)(P_1 - P_2) \\ \quad \Upsilon_{24} \triangleq (V_{20}A_1 + V_{10}A_2)\dot{w} \\ \Xi_2 = \left[V_{10} \quad V_{20} \quad C_{cLi} \quad \left(\frac{4\pi^2}{\eta_V D} C_{pLi} J_{HP}\right)\right]^T \\ \nu_2 = -x_1 x_2 A_1 A_2 (A_1 - A_2)\left(sm(x_2) + sm(-x_2)\right) \end{cases} \tag{46}$$

$$f_3 \Rightarrow \begin{cases} \gamma_3 = K_{dr}(V_{20}A_1 + V_{10}A_2) \\ \Xi_3 = \eta_V D + T_{fHP}\dfrac{4\pi^2 C_{pLi}}{\eta_V D} \\ \nu_3 = 0 \end{cases} \tag{47}$$

$$f_4 \Rightarrow \begin{cases} \gamma_4 = (V_{10} + A_1 x_1)(V_{20} - A_2 x_1) \\ \Xi_4 = \beta^{-1} \\ \nu_4 = 0 \end{cases} \tag{48}$$